Published in final edited form as:
J Comp Neurol. 2012 August 15; 520(12): 2742–2756. doi:10.1002/cne.23084.

Morphology of Axonal Projections From the High Vocal Center to Vocal Motor Cortex in Songbirds

Zhiqi C. Yip, **Vanessa C. Miller-Sims**, and **Sarah W. Bottjer***
Section of Neurobiology, University of Southern California, Los Angeles, California 90089

Abstract

Only birds that learn complex vocalizations have telencephalic brain regions that control vocal learning and production, including HVC (high vocal center), a cortical nucleus that encodes vocal motor output in adult song-birds. HVC projects to RA (robust nucleus of the arco-pallium), a nucleus in motor cortex that in turn projects topographically onto hindbrain neurons innervating vocal muscles. Individual neurons projecting from HVC to RA (HVC_{RA}) fire sparsely to drive RA activity during song production. To advance understanding of how individual HVC neurons encode production of learned vocalizations, we reconstructed single HVC axons inner-vating RA in adult male zebra finches. Individual HVC_{RA} axons were not topographically organized within RA: 1) axon arbors of HVC cell bodies located near each other sent branches to different subregions of RA, and 2) branches of single HVC axons terminated in different locations within RA. HVC_{RA} axons also had a simple, sparse morphology, suggesting that a single HVC neuron activates a limited population of postsynaptic RA neurons. These morphological data are consistent with previous work showing that single HVC_{RA} neurons burst sparsely for a brief period of time during the production of a song, indicating that ensembles of HVC_{RA} neurons fire simultaneously to drive small temporal segments of song behavior. We also examined the morphology of axons projecting from HVC to RA cup, a region surrounding RA that receives input from auditory cortex. Axons projecting to RA cup also sent some branches into RA, suggesting direct integration between the sensory and motor circuits for song control.

Keywords

vocalization; vocal learning; motor pathway

Complex motor behaviors such as running, playing the piano, and producing speech require the brain to execute stereotyped neural sequences. Understanding how the brain comes to control a series of complicated movements is essential for developing treatments for learning disorders and motor dysfunction. In adult male zebra finches (*Taenopygia guttata*), the cortical nucleus HVC (high vocal center; located in the nidopallium; Reiner et al., 2004) generates highly stereotyped and precisely timed activity patterns that control learned vocal output (Nottebohm et al., 1976; Simpson and Vicario, 1990; Vu et al., 1998; Hahnloser et al., 2002; Wild, 2004; Ashmore et al., 2005). The projection from HVC to RA (robust nucleus of the arcopallium; in motor cortex; Fig. 1) provides an interesting model for understanding how sparse firing codes in HVC influence the relatively "dense" firing patterns in RA to control a fixed motor sequence (Yu and Margoliash, 1996; Dave and Margoliash, 2000). HVC receives auditory input indirectly via primary auditory cortex and

*CORRESPONDENCE TO: S.W. Bottjer, University of Southern California, Dept. of Biology, HNB 218, Los Angeles, CA 90089-2520. bottjer@usc.edu.

directly via two higher-level auditory regions of cortex, nucleus interface of the nidopallium (NIf) and caudal mesopallium (CM) (Vates et al., 1996; Cardin and Schmidt, 2004a,b; Coleman and Mooney, 2004; Bauer et al., 2008; Wang et al., 2010; Akutagawa and Konishi, 2010). Individual HVC_{RA} neurons produce brief bursts of action potentials at highly precise times during the production of song as well as when the bird hears its own song played back (Hahnloser et al., 2002, 2006; Prather et al., 2008).

HVC contains two separate populations of projection neurons. One population projects to a basal ganglia pathway necessary for plasticity in vocal behavior (Bottjer 2004; Brainard, 2004). As indicated above, the second population sends axons to the motor-cortical nucleus RA (Nottebohm et al., 1976, 1982; Bottjer et al., 1989; Johnson and Bottjer, 1993, 1995; Foster and Bottjer, 1998), which in turn drives activity in vocal motor and respiratory hindbrain regions to produce stereotyped learned vocal output (Wild, 1993, 2004; Sober et al., 2008) (Fig. 1). The axonal projections of HVC are nontopographic: tracer injections into single subregions of HVC produce a uniform distribution of anterograde label throughout RA rather than in a specific restricted location (Fortune and Margoliash, 1995; Vates and Nottebohm, 1995; Foster and Bottjer, 1998). Interestingly, other projections to and from RA are highly topographic (Vicario, 1991; Johnson et al., 1995; Vates and Nottebohm, 1995). Dorsal RA is innervated by axons from the medial portion of LMAN (lateral magnocellular nucleus of the anterior nidopallium; Fig. 1) and projects to mid- and hindbrain regions that control respiration (Wild, 1993, 2004). Intermediate RA is innervated by intermediate LMAN and projects to rostral hypoglossal motor neurons, which project to ventral muscles of the vocal organ (syrinx); ventral RA is inner-vated by lateral LMAN and projects to caudal hypoglossal motor neurons, which innervate the dorsal muscles of the syrinx (Vicario, 1991). Ventral syringeal muscles control the fundamental frequency of vocalizations and dorsal syringeal muscles control the timing and amplitude of sound production (Goller and Suthers, 1996; Suthers and Zollinger, 2004).

During song production, HVC_{RA} neurons produce a brief burst of spikes at a single point during each rendition of a song motif (Hahnloser et al., 2002; Fee et al., 2004), whereas RA neurons produce ≈10–12 bursts (Yu and Margoliash, 1996; Leonardo and Fee, 2005; Sober et al., 2008). Different combinations of HVC_{RA} neurons burst at different timepoints in the song. This pattern has given rise to a synaptic-chain model for vocal production in which ensembles of HVC_{RA} neurons burst sequentially and trigger the next group of neurons in the sequence to fire (Hahnloser et al., 2002; Fee et al., 2004; Long et al., 2010). This model suggests that different ensembles of HVC_{RA} neurons fire at specific points in the song to control a short segment or subsyllable of song, and that each neuron contributes to only a small proportion of song production. We analyzed the morphological characteristics of single HVC_{RA} axons to determine how connections from HVC to RA are organized. In accord with the idea that single HVC neurons contribute to a brief interlude of the song pattern, HVC_{RA} axons exhibited an extremely simple morphology with limited branching patterns. We also reconstructed axons projecting from HVC to the area surrounding anterior and ventral RA, RA cup (Kelley and Nottebohm, 1979; Vates et al., 1996). RA cup receives inputs both directly and indirectly from auditory cortex and projects to thalamic, midbrain, and pontine nuclei of the ascending auditory pathway (Mello et al., 1998). We found that individual axons projecting to RA cup also extended branches into RA, indicating that sensory and motor integration may occur directly at the level of RA.

MATERIALS AND METHODS

Male adult zebra finches (>90 days; $n = 5$) used in this study were raised by their parents in our¼breeding aviary at the University of Southern California (USC) and thus had normal exposure to song. All experiments were conducted in accordance with National Institutes of

Health guidelines and the Animal Care and Use Committee at USC. Birds were anesthetized with 1.5% isoflurane and placed in a stereotaxic device. A small midline skin incision was made to expose the skull. Stereotaxic coordinates were used to locate the position of HVC. A small piece of skull overlying HVC was removed and a glass pipette (OD 20 μm) filled with 0.5M NaCl was used to make multiunit recordings of spontaneous activity in order to confirm the location of HVC. The pattern of bursting activity characteristic of HVC was used to map its dorsal-ventral extent and to target injections to the middle of HVC.

Biotinylated dextran amine (BDA) injections

A glass pipette (OD 6–8 μm) filled with the anterograde tracer BDA (10,000 MW BDA in 10% sterile-filtered phosphate-buffered saline [PBS], pH 7.4) was lowered into HVC on one side and pulses of positive current were applied to a silver wire for 20 minutes to make iontophoretic injections of BDA (200–400 nA, 1 sec on, 1 sec off). Although all surgeries were targeted bilaterally, in every case only one of the injections was traceable either because the other injection missed or was too big (i.e., too many axons were labeled and individual processes could not be distinguished). Following surgery, birds ($n = 4$) were placed into single cages and returned to the aviary for 2 days. An example of an injection site in HVC with labeled cell bodies is shown in Figure 2A.

Lentivirus production and injections

As an alternate tracer, we used a lentivirus with a chicken beta-actin promoter fused to green fluorescent protein (GFP; gift from Dr. Tansu Celikel). GFP was expressed from a lentiviral vector under control of the cytomegalovirus (CMV)-enhanced chicken beta-actin promoter, FCAGGW. This vector was produced by removing the CAG-GFP cassette from pCAG-GFP (Matsuda and Cepko, 2004; Addgene plasmid 11150) using SpeI and BsrGI, and subcloning this cassette into the lentiviral backbone, derived from FCK-ChR2-GFP (Addgene plasmid 15814; Boyden et al., 2005) cut with XbaI and BsrGI (all enzymes from Fermentas, Burlington, ON, Canada). The lentiviral vector construct was verified by enzymatic digestion, gel electrophoresis, and DNA sequencing (DNA Core Facility, USC). This construct was then mixed with packaging plasmids (psPAX2 and pMD2.G, Addgene plasmids 12260 and 12259, respectively) and used with Lentiphos HT transfection system (ClonTech, Palo Alto, CA) to transfect 293T cells (50–60% confluency) for production of VSV-G pseudotyped, replication-incompetent lenti-virus. The vector map is shown in Figure 3. Viral titers were determined using the p24 antigen enzyme-linked immunosorbent assay (ELISA) kit (ClonTech). Viral packaging and titration were performed by the USC Lentiviral Core Facility. GFP-expressing lentivirus with a titer of 1×10^7 IFU/ml was infused (250–500 nL over 2 min) into HVC using a premarked glass pipette (ID 15–18 μm, OD <45 μm) connected to a 50-mL syringe with Tygon tubing. The bird ($n = 1$) injected with the lentivirus was placed in a cage and housed in the main aviary for 10 days following surgery.

Tissue processing

Following the postsurgery period, birds were deeply anesthetized with the barbiturate anesthetic Equithesin (0.06–0.08 ml / 15–20 g) and perfused through the heart with 0.7% PBS, followed by 4% paraformaldehyde with 0.4% glutaraldehyde (pH 7.8). Brains were postfixed in 4% paraformaldehyde for 24 hours and then cryoprotected in 25% sucrose in PBS for another 24 hours. Brains were frozen-sectioned coronally at a thickness of 50 lm and collected in 0.02M PBS as free-floating sections. Sections were stained using standard immunohistochemical procedures as previously described (Foster et. al., 1997). Sections were washed in PBS three times and pretreated in 1% H_2O_2 in PBS for 30 minutes to quench endogenous peroxidase activity. For the BDA injections, the sections were incubated

in 5% normal rabbit serum (Vector Laboratories, La Jolla, CA) in 0.3% Triton-X for 40 minutes to prevent nonspecific antibody binding, and then incubated overnight in primary antibody (goat antibiotin, 1:20,000, Vector Laboratories). Sections were incubated in secondary antibody (biotinylated antigoat IgG, 1:200) for 1 hour in 0.3% Triton-X followed by avidin-biotin peroxidase rea-gent in 0.3% Triton-X (ABC Elite Kit, Vector Laboratories) for 1 hour. Reaction product was visualized using 0.05% 3,3′-diaminobenzidine (DAB) in PBS. Sections were first preincubated in 0.05% DAB for 15 minutes, then placed in 0.05% DAB plus graduating concentrations of H_2O_2 (0.003% for 5 min, followed by 0.015% for 5 min). The reaction was terminated by washing the sections three times in PBS, following which the tissue was mounted onto gelatin-subbed slides and air-dried. Sections were dehydrated in ethanol, defatted in xylene, and cover-slipped with Permount. The same immunohistochemical procedures were performed for the lentivirus injections except that 5% normal goat serum (Vector Laboratories) was used for the blocking serum, and sections were reacted using anti-GFP primary antibody (rabbit polyclonal serum, 1:2,000, Invitrogen) and secondary biotinylated antirabbit IgG (1:200, Vector Laboratories).

Data analysis

Individual axon arbors of HVC_{RA} neurons were reconstructed in three dimensions under 1,000× final magnification using a light microscope (Leica DMRE) with a motorized stage and Neurolucida software (MicroBrightField, Colchester, VT). We reconstructed axons from left HVC in two BDA-labeled birds (n = 5), right HVC in the other two BDA-labeled birds (n = 6), and right HVC in the GFP-labeled bird (n = 5). Axons within RA were chosen for reconstruction based on whether all branches for a given arbor were completely labeled; only well-labeled axons were traced (Fig. 2B). Markers were placed along the axon at the location of each varicosity (Fig. 2B, arrowheads). Following axon reconstructions, alternate tissue sections were Nissl-stained and the borders of RA were traced to confirm the location of the axon arbors within RA. To correct for shrinkage of the tissue during processing in the z-axis, a correction factor was calculated and applied to the axon tracings in Neurolucida. To calculate the shrinkage correction factor, we measured the thickness of the sections by focusing on the top and bottom surfaces at 1,000× and then dividing the initial thickness of the tissue slices (50 μm) by this number. The mean ± standard deviation correction factor applied to the tissue was 5.26 ± 0.97.

All branches of a single axon arbor were traced, regardless of whether they were located inside or outside of RA. However, we quantified axon arbors only within RA; for HVC_{RA} axons that extended branches outside RA, we detached the portion of the axon outside RA and made measures only of the arbor branches within the borders of RA (see below). We quantified the morphology of HVC_{RA} axons by examining 1) the length, spatial extent, and volume of the axon arbors, 2) the complexity of axonal branching patterns, and 3) the number and distribution of varicosities. (1) We calculated the total length of each axon within RA and mean branch length (a branch is defined as the segment of an axon between branch points) for each axon. To assess how much of RA was encompassed by single HVC axon arbors, we measured the tangential extent of each arbor in the medial-lateral, dorsal-ventral, and anterior-posterior directions as the distance between the point where the axon entered RA to the furthest branch ending in the dorsal-ventral, medial-lateral, and anterior-posterior axes of RA, respectively. This tangential distance was then divided by the maximum cross-sectional distance of RA for each corresponding axis (all distances measured using Free Ruler software, Pascal). We also quantified the volume of each axon arbor and the percent volume of RA encompassed by single axon arbors. The volume occupied by each axon arbor was measured with a 3D convex hull analysis using the Neurolucida program. This analysis generates a convex polygon around the distal-most branch points of each arbor and measures the resultant volume. We then determined the

volume of RA by multiplying the surface area of each section (obtained by tracing the Nissl-defined borders of RA) by the thickness of each tissue section and summing these values. To measure the percent volume encompassed by individual axon arbors we divided the volume of each axon arbor by the volume of RA. (2) We evaluated the complexity of HVC_{RA} axons by measuring the number of branches, number of branch endings (defined as the termination of an axon branch), and highest branch order. The first-order branch emanated from the cell body and ended at the first branch point; second-order branches began at the first branch point and ended at the next branch point, and so on. (3) We measured the total number of varicosities, which represent putative synaptic contacts, the number of varicosities per branch, and varicosity density. Varicosity density was determined by dividing the total number of varicosities by the total length of each axon. We quantified the same measures for axons that projected from HVC into RA cup, a portion of arcopallium that surrounds the borders of RA and receives input directly from layers L1 and L3 of Field L (the analog of mammalian primary auditory cortex) and indirectly via HVC shelf, a band of nidopallium located immediately ventral to HVC (Mello et al., 1998). Several measures were not normally distributed, so we report median values for these dependent measures throughout the article. We performed Mann–Whitney tests to determine if values for BDA- and GFP-labeled axons were significantly different and Friedman (within-subject) tests to determine if there were differences in innervation patterns in different subregions of RA. Image-processing software (Picasa, Google) was used to make slight increases in the brightness and contrast of the photomicro-graphs in Figure 2; all adjustments were applied to the entire image in each case.

RESULTS

HVC_{RA} axons

To characterize the morphology of HVC axons projecting to RA in adult male zebra finches, we reconstructed the arbors of single axons within RA labeled with either BDA or GFP fused to a lentivirus. A total of 16 axons in five birds were reconstructed; 11 axons in four birds were labeled with BDA (Fig 4A–D), and five axons in one bird were labeled with lentivirus fused to GFP (Fig. 4E). We calculated morphological characteristics for BDA- and GFP-labeled axons separately and compared the measurements (Tables 1–3). There was no significant difference between BDA- and GFP-labeled axons in any parameter except varicosity density ($U = 5$, $P = 0.01$; Table 3). Unless noted otherwise below, all descriptions apply to both BDA- and GFP-labeled axons.

We also observed a small number of retrogradely labeled cell bodies in RA: three birds in which HVC was injected with BDA each had one very well-labeled neuron in the dorsal anterior region of RA (an example is shown in Fig. 2C). These well-labeled cell bodies in RA are consistent with the report of Roberts et al. (2008) of a sparse reciprocal connection from RA to HVC.

We began tracing HVC_{RA} axons as they descended ventrally and caudally toward the dorsomedial border of RA. Because injections in two birds also labeled cell bodies outside the borders of HVC (Fig. 4, right column, A–B), we followed all 16 reconstructed axons back to their injection sites in order to see if we could determine whether the parent cell body for each axon was located within HVC. In all, 15 of 16 axons unambiguously originated from within HVC, but we were unable to trace the remaining axon (Fig. 4B, black) back to its parent cell body to determine whether its arbor emanated from within HVC. However, given that this axon arbor ramified only within RA, it is likely that its cell body was located within HVC, although we cannot be certain that the parent cell body was not just outside of or on the borders of HVC.

While most HVC axons branched either within or immediately before entering RA, one axon (Fig. 4D, green) bifurcated ≈800 μm dorsal to RA; however, the entire arbor derived from those two initial branches was confined to RA. In addition, three axons (Fig. 4B, brown; 4C, black; 4E, blue) branched just prior to entering RA. All branches of these arbors were also confined to RA, showing that HVC_{RA} axons that branch prior to entering RA do not arborize in other brain regions. However, two of the 16 axons did extend branches outside RA. One axon (Fig. 4B, red) extended branches that terminated within dorsal RA as well as within Ad (dorsal arcopallium), an arc-shaped region lateral to RA that is necessary for vocal learning in juvenile birds (Bottjer and Altenau, 2010). The other arbor (Fig. 4E, black) contained branches that terminated within RA and one branch that extended ventrally outside RA into RA cup, a region that surrounds the anterior and ventral borders of RA (Mello et al., 1998; see below). All 16 axons tended to have a simple morphology with limited total length and branching; some axons had extremely limited branching patterns (e.g., Fig. 4A, black).

Distribution of single HVC axons within RA is nontopographic—As predicted by earlier work showing a nontopographic pattern of connectivity between subregions of HVC and RA (Fortune and Margoliash, 1995; Vates and Nottebohm, 1995; Foster and Bottjer, 1998), we found that projections of single axons from HVC to RA were nontopographic. Axon arbors of cell bodies located adjacent to one another in HVC branched within different, largely nonoverlapping subregions of RA. We reconstructed three or more HVC_{RA} axons for four different injection sites (Fig. 4B–E), and in each case arbors of neighboring HVC neurons terminated in distinct, nonoverlapping locations within RA. Neurons located in the extreme medial portion of HVC (Fig. 4B) gave rise to one axon that terminated only in the dorsal region of RA (red), one that descended ventrolaterally within RA (black), and one that extended ventrally through central RA (brown). Similarly, labeled cell bodies restricted to central HVC extended axons from dorsal to ventral within central RA (Fig. 4D, red) as well as within medial RA (Fig. 4D,E, green), dorsal RA (Fig. 4E, blue and brown), and central-lateral RA (Fig. 4E, red, black). In addition, single HVC cell bodies gave rise to axon arbors with branches that terminated in different subregions of RA. Out of 16 axons, 10 had branches that ended in different subregions of RA. Of these 10 axons, nine were oriented primarily in the dorsoventral direction and had branch endings in both dorsal and ventral regions of RA (e.g., Fig. 4A,B, black), and one (Fig. 4B, red) terminated in both dorsomedial and dorsolateral RA. Even axons with very simple morphology had branches that terminated far away from each other. For example, axons in Figure 4A,4E (green) each had only three branches, yet had endings located in both dorsomedial and ventral RA. Thus, axonal projections from HVC to RA are not topographically organized, despite the fact that projections from LMAN to RA as well as from RA to downstream motor circuits are topographic (Vicario, 1991; Johnson et al., 1995; Vates and Nottebohm, 1995).

Qualitative examination of Figure 4 suggests that many HVC arbors did not extend branches into ventral RA, or that arbors that branched in dorsal and central regions of RA extended only a single branch into ventral RA. In order to assess this trend quantitatively, we divided RA into dorsal, middle, and ventral sections and measured what proportion of the total length, varicosities, and branch endings for each axon were located within each section (Fig. 5). These data showed a steep decrease in all three measures along the dorsal-ventral axis of RA ($P < 0.01$ in all cases). The density of varicosities within each section of RA was not different (mean number of varicosities/mm was 51, 62, and 67 in dorsal, middle, and ventral RA, respectively; $P > 0.50$), confirming that this pattern was due to fewer axonal branches extending into ventral RA. This pattern was also observed by Kittelberger (2002), and seems surprising since it indicates that the overall density of innervation from HVC is lower in ventral RA. Interestingly, the dorsal-ventral axis is the primary axis of topographic organization within RA, and corresponds to the functional representation of respiratory and

vocal muscles (i.e., to the topographic projections from RA to downstream vocal motor circuits) (Vicario, 1991; Suthers and Zollinger 2004; Wild, 2004).

HVC_{RA} arbors can extend throughout RA but do not occupy a large volume— We quantified the total length, average branch length, tangential extent (measured as the maximum distance of each arbor in the dorsal-ventral, medial-lateral, and anterior-posterior axes), and volume of each axon arbor within the borders of RA (Table 1). The total length across all HVC_{RA} axons was 1.57 ± 0.42 (median ± SEM) mm, and the median of average branch length was 0.19 ± 0.05 mm. The tangential extent of axon arbors occupied ≈0.3–0.5 mm in each axis. These values were divided by the maximum length of the corresponding axis to yield the percentage of each axis occupied by the tangential length for each axon (see Materials and Methods); the median values ranged from 38% of the anterior-posterior axis to 61% of the dorsal-ventral axis (Table 1). Thus, although individual axons have a simple morphology, they extend across a substantial proportion of each axis of RA. The median volume of axon arbors within RA was 0.0045 ± 0.004 mm^3. The percentage of RA encompassed by each axon arbor, calculated by dividing the volume of each arbor by the total volume of RA, was 1.75 ± 1.66%. Previous work from our laboratory has shown that thalamic axon arbors occupy ≈4% of $LMAN_{core}$ volume, and $LMAN_{core}$ axons occupy ≈9–10% of the volume of RA (Iyengar and Bottjer, 2002; Miller-Sims and Bottjer, 2012). Thus, despite terminating in different subregions of RA, individual HVC axon arbors occupy a substantially smaller proportion of RA than do single axons emanating from $LMAN_{core}$.

Despite the fact that individual HVC axons encompassed a very small proportion of postsynaptic space in RA, a few axons from a single injection site in HVC nevertheless covered a large portion of RA due to the nontopo-graphic projections of single axons. We calculated the total combined volume of all arbors for three injection sites that each had 3–5 reconstructed axons (Fig. 4B,D,E). On average, the reconstructed axons covered 47 ± 11% of RA.

HVC_{RA} axons exhibit a limited branching pattern

HVC_{RA} axon arbors tended to show a very sparse pattern of branching (Fig. 4). To assess the complexity of branching patterns, we calculated the highest branch order (tiers of branching), number of branch endings, and number of branches. The median highest branch order was 4.5 ± 0.6 (Table 2). The 16 axons had between 1 and 26 endings with a median value of 5.0 ± 1.5 endings per axon, and the number of branches ranged from 1 to 52 with a median value of 9.0 ± 3.1, suggesting that HVC_{RA} axons as a population have simple branching patterns.

Figure 6A shows the frequency distribution of all axons as a function of highest branch order. Seven out of 16 axons had three tiers of branches or fewer, suggesting that a subpopulation of HVC_{RA} axons had an extremely simple branching pattern. One axon (Fig. 4C, brown) did not branch at all; its single branch traversed the dorsal and medial portions of RA. The remaining axons had up to nine tiers of branches (Fig. 6A). We also examined the mean number of branches by branch order (Fig. 6B). Across all axons the greatest number of branches occurred at the third order of branching, and number of branches decreased with increasing orders of branching. Only one axon had ninth-order branches across all 16 axons (although that axon had six ninth-order branches; Fig. 4D, red). To underscore the point that HVC axons in RA have simple branching patterns, Figure 6C shows the number of branches by branch order as a percentage of the maximum number of branches possible for each branch order. (The maximum number of branches in each branch order is 2^{n-1} where n is branch order number; the greatest number of branches possible is therefore 1 for the first order of branching, 2 for the second order, 4 for the third order, and so on.) The percentage of possible branches started out at 94–100% for first- and second-

order branches, dropped to 56% for the third tier of branches, and declined to 19% for fourth-order branches. Thus, the percent of possible maximum branches declined steeply and was less than 10% for fifth-order branch orders and above, showing that axons divide into branches much less frequently at higher branch orders. We also examined the length of branches as a function of branch order (Fig. 6D). Branch length was roughly equivalent over the first six orders of branching, but was shorter at the highest levels of branching (for the five arbors that had branches with seven or more tiers of branching; cf. Fig. 6A). Altogether, these measures show that most HVC axons display a highly sparse branching pattern in RA.

Varicosities of HVC_{RA} axons are distributed evenly across the arbor—Half of all HVC axons (8/16) had varicosities just prior to entering RA, suggesting that HVC_{RA} axons make synapses in the region just dorsal to RA, which may include RA cup. Varicosities first appeared ≈200 μm dorsal to RA, and no axon had more than four varicosities before entering RA. As noted above, BDA-labeled axons had many more varicosities than did GFP-labeled axons (Table 3). The reason for this discrepancy is unclear. The median number of varicosities per branch for BDA-labeled axons was 10.0 ± 4.1, and the varicosity density was 53.9 ± 6.3. We plotted median varicosity density as a function of branch order in order to determine whether varicosities were distributed evenly across each axon arbor; this analysis was restricted to the 11 BDA-labeled axons (Fig. 7). Across all branches of BDA-labeled axons, the varicosity density was lowest at the first order of branching and was distributed approximately evenly over the second through eighth levels of branching. The density of varicosities was higher at the ninth level of branching, but this value represented only one axon (Fig. 6A), and some of its ninth-order branches were extremely short, which artificially inflated the median value for varicosity density. These data show that varicosity density did not change appreciably as a function of branch order.

Axons in RA cup

We also traced five BDA-labeled axons that projected to a region that surrounds the borders of RA, known as the RA cup (Kelley and Nottebohm, 1979). This area receives auditory inputs both directly from layers L1 and L3 of auditory cortex and the caudal mesopallium (CM) and indirectly via the shelf region just ventral to HVC (Mello, et al., 1996, 1998). These five RA cup axons originated from an injection site that encompassed medial HVC and lateral paraHVC, a caudomedial extension of HVC containing neurons that project to Area X in the striatum (Johnson et al., 1995) (Fig. 8); we did not trace any of the axons projecting only into RA for this site. The injection did not appear to include HVC shelf, an area immediately ventral to the borders of HVC and paraHVC. Like HVC_{RA} axons, RA cup axons ranged from very simple axons (four very short branches for the green axon) to more complex (25 branches for the black axon). The axons entered dorsal RA cup and sent branches that arborized primarily anterior to RA, in ventrolateral RA cup. The black axon also sent some branches into anterior dorsomedial RA cup (Fig. 8), and the blue axon arborized primarily in the dorsal region of anterior RA cup. Two out of the five axons reconstructed in RA cup also extended several branches into RA; the black axon extended seven branches with varicosities into dorsomedial anterior RA, and the blue axon extended 11 branches with varicosities that seemed to enter RA, although it was difficult to be certain whether all these latter branches were located within RA since they tended to travel along the mid-anterior border of RA. These data indicate that individual axons coming from HVC can arborize within both RA and RA cup.

We examined RA cup qualitatively in the five birds shown in Figure 4 in order to determine whether these injection sites also gave rise to axons in RA cup. Two of these five injection sites gave rise to many labeled axon branches in RA cup (Fig. 4A,B), an additional two

injection sites produced a small number of branches in RA cup (Fig. 4C,E), and the remaining injection site produced very few branches in RA cup (Fig. 4D). Overall, these results show that neurons within the borders of HVC can send axonal branches directly to both RA and RA cup.

Quantitative analysis of axons within RA cup is summarized in Table 4. The median total length was 1.60 ± 0.58 mm, and the median for average branch length was 0.23 ± 0.03 mm; these values are very similar to those for HVC arbors within RA. The highest branch order was 4.0 ± 1.0, the number of branches was 7.0 ± 3.1, and the number of branch endings was 4.0 ± 1.6. RA cup axons had 6.0 ± 2.1 varicosities in axon segments ≈400 μm prior to the first branch point within RA cup. Since the borders of RA cup are not distinct, we could not determine whether some of these varicosities occur just dorsal to RA cup. The median number of varicosities per branch was 9.9 ± 1.7, and the median varicosity density was 41.8 ± 6.4 varicosities/mm.

DISCUSSION

The majority of HVC_{RA} axons had an extremely simple morphology. Single arbors were limited in total length and number of branches and thus exhibited a simple pattern of branching that occupied a limited proportion of postsynaptic space in RA. In addition, the projections from HVC to RA were nontopographic in two ways: 1) axon arbors of adjacent somata in HVC ramified within different subregions of RA; for example, the arbor of one HVC neuron terminated in medial RA while the arbor of a neighboring HVC neuron terminated in dorsal, lateral, and ventral RA (red and green axons, respectively, in Fig. 4D); and 2) branches of single HVC_{RA} axon arbors terminated in different locations within RA (e.g., red axons in Fig. 4D,E). Because both single arbors and individual branches within an arbor frequently encompassed different subregions of RA, as few as 3–4 arbors occupied a relatively large proportion of postsynaptic space in RA.

These data show that extremely simple axonal arbors of single cortical neurons can control complex learned motor patterns as a population. The term “cortex” is used here generically in the sense described by Reiner et al. (2004) as including that part of the telencephalon that is “pallial in nature and therefore homologous as a field to the brain region of mammals that includes the neocortex, claustrum, and pallial amygdala” (p. 395). Thus, cortex is derived embryologically from pallium, reflecting its evolutionary origin across major vertebrate taxa (Karten, 1991, 1997; Northcutt and Kaas, 1995; Swanson, 2000; Jarvis et al., 2005). In addition, axonal connections of cortex and expression patterns of neurotransmitters are broadly conserved across vertebrate taxa, and the functions impaired by cortical damage are those having to do with high-level aspects of perception, learning, and memory (Reiner et al., 2005; Butler et al., 2011). Thus, avian brains meet developmental-evolutionary-functional criteria for having a cortex, although it is likely to be organized differently from mammalian cortex. Our usage of the term “cortex” has no implications for direct homologies between specific regions of avian and mammalian brain, as one-to-one homologies have yet to be established with certainty.

HVC_{RA} neurons: simple axonal morphology and the sparse code during singing

The simplicity of HVC_{RA} axons is consistent with the fact that individual HVC_{RA} neurons burst in a highly sparse pattern during song and hence code for very brief segments of the song motif (Hahnloser et al., 2002; Fee et al., 2004). The sparse code seen in HVC_{RA} neurons is translated into a relatively dense pattern of bursting in RA, since individual RA neurons burst several times during a song motif (Yu and Margoliash, 1996; Dave and Margoliash, 2000; Chi and Margoliash, 2001; Leonardo and Fee 2005; Sober et al., 2008). In both HVC and RA, action potential bursts are very precisely correlated with specific

timepoints during song production. Together, the morphological and electrophysiological data suggest that single HVC axons drive a limited number of RA neurons at a unique timepoint, but that individual RA neurons receive convergent input from many HVC neurons in order to drive single RA neurons at multiple points in the song. This scenario is consistent with the idea of a synaptic-chain model in which different subpopulations of HVC_{RA} neurons burst sequentially during a song motif to drive brief sequences of stereotyped vocal output (Fee et al., 2004; Leonardo and Fee, 2005; Li and Greenside, 2006; Jin et al., 2007; Long et al., 2010).

Compared to LMAN axons that innervate RA, individual HVC_{RA} axons are much less extensive in total length and number of branches, and have fewer branch orders. In addition, HVC_{RA} arbors have a much smaller volume than $LMAN_{RA}$ arbors, and hence occupy a substantially smaller percentage of RA; HVC axons occupy ≈2% of the postsynaptic space in RA compared to ≈10% for LMAN axons (Miller-Sims and Bottjer, 2012). Despite this fact, the tangential extent of arbors within RA is not significantly different between axons from HVC and those from LMAN. In addition, HVC_{RA} axons have a much higher density of varicosities compared to $LMAN_{RA}$ axons (roughly four times as many varicosities/mm). Estimates of the number of projection neurons in adult male zebra finches indicate that HVC has approximately six times as many RA-projecting neurons as does LMAN (Nordeen and Nordeen, 1988; Nordeen et al., 1992). This pattern suggests that single axons from subgroups of adjacent HVC neurons make a high density of synaptic contacts on a limited number of neurons located in different subregions of RA, whereas axons from subgroups of adjacent LMAN neurons make relatively fewer synapses within the same subregion of RA (cf. Canady et al., 1988; Mooney, 1992). An intriguing possibility is that the nontopographic inputs from HVC are integrated with the topographic pattern of LMAN inputs to RA via this system of overlapping inputs, in conjunction with the rich plexus of internal connections within RA (Herrmann and Arnold, 1991; Spiro et al., 1999). Such integration may form an essential aspect of transforming a temporal population code (in HVC) to a map-based motor code (in RA and hindbrain motor circuits).

Morphology of HVC_{RA} axons and generation of a complex vocal repertoire

How might the morphological pattern of HVC_{RA} axons contribute to vocal output? It is possible that some constant number of RA neurons must be activated by an ensemble of HVC_{RA} neurons to drive output of a brief vocal sequence (Sober et al., 2008). If so, then having sparse HVC_{RA} axons (thus contacting fewer postsynaptic RA neurons) means that more HVC_{RA} axons per ensemble are required to drive each sequence. That is, a relatively large population of sparsely branched HVC_{RA} axons would be required to produce a small segment of song such that each HVC_{RA} neuron would make only a small contribution to the activity of the population. One caveat is that the morphology of HVC_{RA} axons shown in Figure 4 was fairly variable, with some axons having a highly simple morphology and others having more branches and covering a larger extent. We do not know whether HVC_{RA} neurons represent a homogeneous functional population; for example, individual neurons in this identified class may vary depending on what afferent inputs they receive, their intrinsic pattern of connectivity, and their specific postsynaptic targets in RA and/or RA cup. For example, it is not known whether individual RA projection neurons output to common postsynaptic targets (including both vocal motor neurons and respiratory neurons; see below), or whether different classes of RA neurons synapse on unique classes of postsynaptic neurons. In the latter case, it may be that the morphology of HVC_{RA} axons depends on the class of RA projection neuron that is contacted.

One potential advantage of simple HVC_{RA} axons is that they could produce a larger repertoire of sounds than the same number of axons with a complex branching pattern. For example, in an imaginary population of 12 RA neurons, if 10 are required to drive a segment

of song, then there are 66 possible combinations of activation patterns in RA, which could produce 66 distinct sounds (i.e., the mathematical combination 12 choose 10 = 66). If we assume that each HVC axon contacts a single RA neuron, then as few as 12 HVC_{RA} axons are required to activate all 66 combinations of 10 neurons. In contrast, if each HVC axon contacts 10 RA neurons (e.g., each axon has 10 branches, each of which contacts a different RA neuron), then 66 HVC_{RA} axons would be needed to produce 66 different sounds. Thus, a simple branching pattern requires fewer HVC_{RA} axons since a small number of axons can combine with one another to produce different patterns of activation in RA and give rise to a large number of distinct sounds.

Previous estimates of the number of RA neurons that are activated during brief song sequences vary from 12–60% (Fee et al., 2004; Sober et al., 2008). If we assume that 400 RA neurons out of a population of 1,000 are required to produce a brief segment of sound, then we can easily calculate how many different combinations of sound are produced depending on how many RA neurons are contacted by a single HVC axon. Figure 9 presents a plot of the number of different sound combinations generated (log values, y-axis) as the number of RA neurons contacted by a single HVC axon increases from 1 to 25 (x-axis). This plot shows that the number of possible sound combinations drops steeply as HVC axons contact a larger number of RA neurons. This simple model makes clear that a population of HVC_{RA} neurons with simple axonal morphology could use a combinatorial code to specify segments of sound, expanding the range of syllables that can be produced. Furthermore, the model is consistent with the sparse bursting pattern of HVC_{RA} neurons, which lasts for only a brief segment of song behavior (≈6 ms; Hahnloser et al., 2002), and thus requires a large number of different combinatorial patterns to code for a large number of unique timepoints in the RA sequence.

One consideration is that even if single HVC axons contact a limited number of postsynaptic RA neurons, the influence of an individual HVC neuron might be much greater if firing patterns in RA are highly correlated (Spiro et al., 1999; Sober et al., 2008). For example, an ensemble of HVC neurons might drive only a small proportion of RA neurons during a brief interval of song, but if the activity of RA neurons covaries (for example, due to patterns of intrinsic connectivity; Herrmann and Arnold, 1991; Spiro et al., 1999), then individual HVC neurons could exert a relatively strong premotor influence over vocal output. Furthermore, convergence of ensembles of HVC_{RA} neurons onto interneurons within HVC could code for longer sequences of vocal output (Yu and Margoliash, 1996).

Pattern of HVC-RA innervation in relation to phonology

An unexpected aspect of our results is that most axons tended to branch more within dorsal and central RA, and to send fewer branches into ventral RA. The percentages of total length, varicosities, and branch endings for BDA-labeled axons were lowest in ventral RA (Fig. 5). The absolute value of total mean length in each section of RA was 1.06, 0.83, and 0.27 mm (for dorsal, middle, and ventral sections, respectively) and the mean absolute number of varicosities from dorsal to ventral RA was 44, 42, and 18. The density of varicosities in ventral RA was slightly higher (for those axons that extended branches into ventral RA), although this difference was not significant (see Results). The dorsal portion of RA projects to midbrain regions that control respiration including DM (dorsome-dial nucleus of the intercollicular complex), RAm (retroambigual nucleus), and PAm (parambigual nucleus) (Wild 1993, 2004). The ventral two-thirds of RA projects to the tracheosyringeal portion of the hypoglossal nucleus (nXIIts) which controls the vocal organ (syrinx). Within this latter region, the intermediate portion of RA projects to the rostral portion of nXIIts, which innervates the ventral muscles of the syrinx; the ventral portion of RA projects to the caudal portion of the nXIIts, which innervates the dorsal muscles of the syrinx (Vicario, 1991). The ventral syringeal muscles control the fundamental frequency of vocalizations and the dorsal

syringeal muscles control the timing of sound production for each side of the syrinx independently to influence the timing and amplitude of phonation (Goller and Suthers, 1996; Suthers and Zollinger, 2004). The pattern of results shown in Figure 5 is consistent with the fact that the dorsal muscle mass is smaller than the ventral muscle mass, but nevertheless suggests that the dorsal muscles of the syrinx require fewer inputs from RA (and hence from HVC) to control onsets and offsets of song syllables. Although we cannot rule out the possibility that ventral RA receives afferent inputs from other sources, our results suggest the possibility that fine aspects of phonology (controlled by the ventral vocal muscles) require a relatively larger contribution of processing power from RA than do onsets and offsets of syllables (controlled by dorsal muscles).

Another interesting aspect of these results is that although single axons sent fewer branches into ventral RA, many arbors traversed the entire dorsoventral extent of RA (Fig. 4). Thus, despite the apparent functional subdivision of RA into “respiratory” (dorsal one-third) and “vocal motor” (ventral two-thirds) regions, single HVC_{RA} axons seem to contact postsynaptic neurons throughout RA, which could provide one means of integrating respiratory and vocal motor control.

Acknowledgments

We thank Tansu Celikel and Florian Freudenberg for providing the lentiviral vector and for help with the lentiviral injections. We thank Eric Fortune for comments on the article.

Grant sponsor: National Institutes of Health; Grant number: NS037547.

LITERATURE CITED

Akutagawa E, Konishi M. New brain pathways found in the vocal control system of a songbird. J Comp Neurol. 2010; 518:3086–3100. [PubMed: 20533361]

Ashmore RC, Wild JM, Schmidt MF. Brainstem and fore-brain contributions to the generation of learned motor behaviors for song. J Neurosci. 2005; 25:8543–8554. [PubMed: 16162936]

Bauer EE, Coleman MJ, Roberts TF, Roy A, Prather JF, Mooney R. A synaptic basis for auditory-vocal integration in the songbird. J Neurosci. 2008; 28:1509–1522. [PubMed: 18256272]

Bottjer SW. Developmental regulation of basal ganglia circuitry during the sensitive period for vocal learning in songbirds. Ann N Y Acad Sci. 2004; 1016:395–415. [PubMed: 15313787]

Bottjer SW, Altenau B. Parallel pathways for vocal learning in basal ganglia of songbirds. Nat Neurosci. 2010; 13:153–155. [PubMed: 20023650]

Bottjer SW, Halsema KA, Brown SA, Miesner EA. Axonal connections of a forebrain nucleus involved with vocal learning in zebra finches. J Comp Neurol. 1989; 279:312–326. [PubMed: 2464011]

Boyden ES, Zhang F, Bamberg E, Nagel G, Deisseroth K. Millisecond-timescale, genetically targeted optical control of neural activity. Nat Neurosci. 2005; 9:1263–1268. [PubMed: 16116447]

Brainard MS. Contributions of the anterior forebrain pathway to vocal plasticity. Ann N Y Acad Sci. 2004; 1016:377–394. [PubMed: 15313786]

Butler AB, Reiner A, Karten HJ. Evolution of the amniote pallium and the origins of mammalian neocortex. Ann N Y Acad Sci. 1225:14–27. [PubMed: 21534989]

Canady RA, Burd GD, DeVoogd TJ, Nottebohm F. Effect of testosterone on input received by an identified neuron type of the canary song system: a Golgi/electron microscopy/degeneration study. J Neurosci. 1988; 8:3770–3784. [PubMed: 2461435]

Cardin JA, Schmidt MF. Noradrenergic inputs mediate state dependence of auditory responses in the avian song system. J Neurosci. 2004a; 24:7745–7753. [PubMed: 15342742]

Cardin JA, Schmidt MF. Auditory responses in multiple sensorimotor song system nuclei are co-modulated by behavioral state. J Neurophysiol. 2004b; 91:2148–2163. [PubMed: 14724261]

Cardin JA, Raksin JN, Schmidt MF. Sensorimotor nucleus Nif is necessary for auditory processing but not vocal motor output in the avian song system. J Neurophysiol. 2005; 93:2157–2166. [PubMed: 15590726]

Chi Z, Margoliash D. Temporal precision and temporal drift in brain and behavior of zebra finch song. Neuron. 2001; 32:899–910. [PubMed: 11738034]

Coleman MJ, Mooney R. Synaptic transformations underlying highly selective auditory representations of learned birdsong. J Neurosci. 2004; 33:7251–7265. [PubMed: 15317851]

Dave AS, Margoliash D. Song replay during sleep and computational rules for sensorimotor vocal learning. Science. 2000; 290:812–816. [PubMed: 11052946]

Fee MS, Kozhevnikov AA, Hahnloser RHR. Neural mechanisms of vocal sequence generation in the songbird. Ann N Y Acad Sci. 2004; 1016:153–170. [PubMed: 15313774]

Fortune ES, Margoliash D. Parallel pathways and convergence onto HVc and adjacent neostriatum of adult zebra finches (Taeniopygia guttata). J Comp Neurol. 1995; 360:413–414. [PubMed: 8543649]

Foster EF, Bottjer SW. Axonal connections of the High Vocal Center and surrounding cortical regions in juvenile and adult male zebra finches. J Comp Neurol. 1998; 397:118–138. [PubMed: 9671283]

Foster EF, Mehta RP, Bottjer SW. Axonal connections of the medial magnocellular nucleus of the anterior neostriatum in zebra finches. J Comp Neurol. 1997; 382:364–381. [PubMed: 9183699]

Glaze CM, Troyer TW. Temporal structure in zebra finch song: implications for motor coding. J Neurosci. 2006; 26:991–1005. [PubMed: 16421319]

Glaze CM, Troyer TW. Behavioral measurements of a temporally precise motor code for birdsong. J Neurosci. 2007; 27:7631–7639. [PubMed: 17634357]

Goller F, Suthers RA. Role of syringeal muscles in controlling the phonology of bird song. J Neurophysiol. 1996; 76:287–300. [PubMed: 8836225]

Hahnloser RHR, Kozhevnikov AA, Fee MS. An ultra-sparse code underlies the generation of neural sequences in a songbird. Nature. 2002; 419:65–70. [PubMed: 12214232]

Hahnloser RH, Kozhevnikov AA, Fee MS. Sleep-related neural activity in a premotor and a basal-ganglia pathway of the songbird. J Neurophysiol. 2006; 96:794–812. [PubMed: 16495362]

Herrmann K, Arnold AP. The development of afferent projections to the robust archistriatal nucleus in male zebra finches: a quantitative electron microscopic study. J Neurosci. 1991; 11:2063–2074. [PubMed: 2066775]

Iyengar S, Bottjer SW. Development of individual axon arbors in a thalamocortical circuit necessary for song learning in zebra finches. J Neurosci. 2001; 22:901–911. [PubMed: 11826119]

Iyengar S, Viswanathan SS, Bottjer SW. Development of topography within song control circuitry of zebra finches during the sensitive period for song learning. J Neurosci. 1999; 19:6037–6057. [PubMed: 10407041]

Jarvis ED, Gunturkun O, Bruce L, Csillag A, Karten H, Kuenzel W, Medina L, Paxinos G, Perkel DJ, Shimizu T, Striedter G, Wild JM, Ball GF, Dugas-Ford J, Durand SE, Hough GE, Husband S, Kubikova L, Lee DW, Mello CV, Powers A, Siang C, Smulders TV, Wada K, White SA, Yamamoto K, Yu J, Reiner A, Butler AB. Avian brains and a new understanding of vertebrate brain evolution. Nat Rev Neurosci. 2005; 6:151–159. [PubMed: 15685220]

Jin DZ, Ramazanoglu FM, Seung HS. Intrinsic bursting enhances the robustness of a neural network model of sequence generation by avian brain area HVC. J Comput Neurosci. 2007; 23:283–299. [PubMed: 17440800]

Johnson F, Bottjer SW. Hormone-induced changes in identified cell populations of the higher vocal center in male canaries. J Neurobiol. 1993; 24:400–418. [PubMed: 8492114]

Johnson F, Bottjer SW. Differential estrogen accumulation among populations of projection neurons in the higher vocal center of male canaries. J Neurobiol. 1995; 26:87–108. [PubMed: 7714528]

Johnson F, Sablan MM, Bottjer SW. Topographic organization of a forebrain pathway involved with vocal learning in zebra finches. J Comp Neurol. 1995; 358:260–278. [PubMed: 7560286]

Karten HJ. Homology and evolutionary origins of the ‘neocortex’. Brain Behav Evol. 1991; 38:264–272. [PubMed: 1777808]

Karten HJ. Evolutionary developmental biology meets the brain: the origins of mammalian cortex. Proc Natl Acad Sci U S A. 1997; 94:2800–2804. [PubMed: 9096300]

Kelley DB, Nottebohm F. Projections of a telencephalic auditory nucleus-field L-in the canary. J Comp Neurol. 1979; 183:455–469. [PubMed: 759444]

Kittelberger, JM. Thesis. Duke University; Durham, NC: 2002. Neurotrophins, synaptic connectivity, and the regulation of song plasticity in the zebra finch..

Leonardo A, Fee MS. Ensemble coding of vocal control in birdsong. J Neurosci. 2005; 25:652–661. [PubMed: 15659602]

Li M, Greenside H. Stable propagation of a burst through a one-dimensional homogenous excitatory chain model of songbird nucleus HVC. Phys Rev E Stat Nonlin Soft Matter Phys. 2006; 74:011918. [PubMed: 16907138]

Long MA, Fee MS. Using temperature to analyse temporal dynamics in the songbird motor pathway. Nature. 2008; 456:189–194. [PubMed: 19005546]

Long MA, Jin DZ, Fee MS. Support for a synaptic chain model of neuronal sequence generation. Nature. 2010; 468:394–399. [PubMed: 20972420]

Matsuda T, Cepko CL. Electroporation and RNA interference in the rodent retina in vivo and in vitro. Proc Natl Acad Sci U S A. 2004; 101:16–22. [PubMed: 14603031]

Mello CV, Vates GE, Okuhata S, Nottebohm F. Descending auditory pathways in the adult male zebra finch (Taeniopygia guttata). J Comp Neurol. 1998; 395:137–160. [PubMed: 9603369]

Miller-Sims VC, Bottjer SW. Auditory experience refines basal ganglia inputs to motor cortex via re-mapping of single axons during the sensitive period for vocal learning in a songbird. J Neurophysiol. 2012; 107:1142–1156. [PubMed: 22157116]

Mooney R. Synaptic basis for developmental plasticity in a birdsong nucleus. J Neurosci. 1992; 12:2464–2477. [PubMed: 1351935]

Mooney R, Prather JF. The HVC microcircuit: the synaptic basis for interactions between song motor and vocal plasticity pathways. J Neurosci. 2005; 25:1952–1964. [PubMed: 15728835]

Nordeen KW, Nordeen EJ. Projection neurons within a vocal motor pathway are born during song learning in zebra finches. Nature. 1988; 334:149–151. [PubMed: 3386754]

Nordeen EJ, Grace A, Burek MJ, Nordeen KW. Sex-dependent loss of projection neurons involved in avian song learning. J Neurobiol. 1992; 23:671–679. [PubMed: 1279116]

Northcutt RG, Kaas JH. The emergence and evolution of mammalian neocortex. Trends Neurosci. 1995; 18:373–379. [PubMed: 7482801]

Nottebohm F, Stokes TM, Leonard CM. Central control of song in the canary, Serinus canarius. J Comp Neurol. 1976; 165:457–486. [PubMed: 1262540]

Nottebohm F, Kelley DB, Paton JA. Connections of vocal central nuclei in the canary telencephalon. J Comp Neurol. 1982; 207:344–357. [PubMed: 7119147]

Prather JF, Mooney R. The HVC microcircuit: the synaptic basis for interactions between song motor and vocal plasticity pathways. J Neurosci. 2005; 25:1952–1964. [PubMed: 15728835]

Prather JF, Peters S, Nowicki S, Mooney R. Precise auditory-vocal mirroring in neurons for learned vocal communication. Nature. 2008; 451:305–310. [PubMed: 18202651]

Reiner A, Perkel DJ, Bruce LL, Butler AB, Csillag A, Kuenzel W, Medina L, Paxinos G, Shimizu T, Striedter G, Wild M, Ball GF, Durand S, Gunturkun O, Lee DW, Mello CV, Powers A, White SA, Hough G, Kubikova L, Smulders TV, Wada K, Dugas-Ford J, Husband S, Yamamoto K, Yu J, Siang C, Jarvis ED. Revised nomenclature for avian telencephalon and some related brainstem nuclei. J Comp Neurol. 2004; 473:377–414. [PubMed: 15116397]

Reiner A, Yamamoto K, Karten HJ. Organization and evolution of the avian forebrain. Anat Rec A Discov Mol Cell Evol Biol. 2005; 287:1080–1102. [PubMed: 16206213]

Roberts TF, Klein ME, Kubke MF, Wild JM, Mooney R. Telencephalic neurons monosynaptically link brainstem and forebrain premotor networks necessary for song. J Neurosci. 2008; 28:3479–3489. [PubMed: 18367614]

Simpson HB, Vicario DS. Brain pathways for learned and unlearned vocalizations differ in zebra finches. J Neurosci. 1990; 10:1541–1556. [PubMed: 2332796]

Sober SJ, Wohlgemuth MJ, Brainard MS. Central contributions to acoustic variation in birdsong. J Neurosci. 2008; 28:10370–10379. [PubMed: 18842896]

Spiro JE, Dalva MB, Mooney R. Long-range inhibition within the zebra finch song nucleus RA can coordinate the firing of multiple projection neurons. J Neurophysiol. 1999; 81:3007–3020. [PubMed: 10368416]

Suthers RA, Zollinger SA. Producing song: the vocal apparatus. Ann N Y Acad Sci. 2004; 1016:109–129. [PubMed: 15313772]

Swanson LW. What is the brain? Trends Neurosci. 2000; 23:519–527. [PubMed: 11074261]

Vates GE, Nottebohm F. Feedback circuitry within a song-learning pathway. Proc Natl Acad Sci U S A. 1995; 92:5139–5143. [PubMed: 7761463]

Vates GE, Broome BM, Mello CV, Nottebohm F. Auditory pathways of caudal telencephalon and their relation to the song system of adult male zebra finches. J Comp Neurol. 1996; 366:613–642. [PubMed: 8833113]

Vicario DS. Organization of the zebra finch song control system: II. Functional organization of outputs from nucleus robustus archistriatalis. J Comp Neurol. 1991; 309:486–494. [PubMed: 1655832]

Vu ET, Schmidt MF, Mazurek ME. Interhemispheric coordination of premotor neural activity during singing in adult zebra finches. J Neurosci. 1998; 18:9088–9098. [PubMed: 9787012]

Wang Y, Brzozowska-Prechtl A, Karten HJ. Laminar and columnar auditory cortex in avian brain. Proc Natl Acad Sci U S A. 2010; 107:12676–12681. [PubMed: 20616034]

Wild JM. Descending projections of the songbird nucleus robustus archistrialis. J Comp Neurol. 1993; 338:225–241. [PubMed: 8308169]

Wild JM. Functional neuroanatomy of the sensorimotor control of singing. Ann N Y Acad Sci. 2004; 1016:438–462. [PubMed: 15313789]

Yu AC, Margoliash D. Temporal hierarchical control of singing in birds. Science. 1996; 273:1871–1875. [PubMed: 8791594]

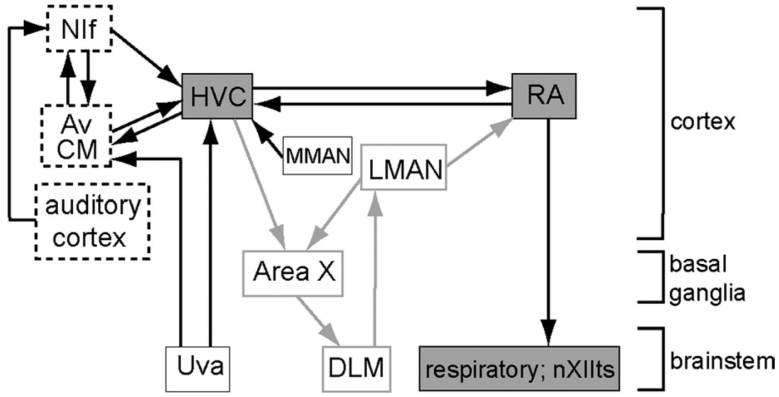

Figure 1.

Schematic of song-control pathways in adult zebra finches. Song-control circuits include the HVC-RA vocal motor pathway in adult birds (boxes shaded gray) and a cortico-basal ganglia-thalamo circuit that is necessary for vocal plasticity (LMAN→Area X→DLM; boxes, gray outline). One population of projection neurons in HVC (HVC_{RA}) sends axonal projections to RA in motor cortex, which in turn drives activity in hypoglossal motor neurons (nXIIts) and respiratory areas in the hindbrain to produce vocal output. Boxes with dashed lines indicate cortical regions with robust auditory responses to vocal sounds that provide input to HVC. The box titled “auditory cortex” includes the thalamorecipient region of primary auditory cortex and adjacent regions, known collectively as the “Field L” complex in avian brain (Wang et al., 2010). Av is a subregion contained within CM (Akutagawa and Konishi, 2010). It should be noted that both NIf and CM/Av may be at least partly sensorimotor in nature (Cardin et al., 2005; Bauer et al., 2008). The term “cortex” is used here generically in the sense described by Reiner et al. (2004; see Discussion). Area X, Area X of the medial striatum (which includes both striatal and pallidal components); Av, nucleus avalanche; CM, caudal mesopallium; DLM, medial dorsolateral nucleus of the thalamus; HVC, high vocal center; LMAN, lateral magnocellular nucleus of the anterior nidopallium; MMAN, medial magnocellular nucleus of the anterior nidopallium; NIf, nucleus interface of the nidopallium; nXIIts, tracheosyringeal portion of the hypoglossal nucleus; RA, robust nucleus of the arcopallium; Uva, uvaeform nucleus of the thalamus.

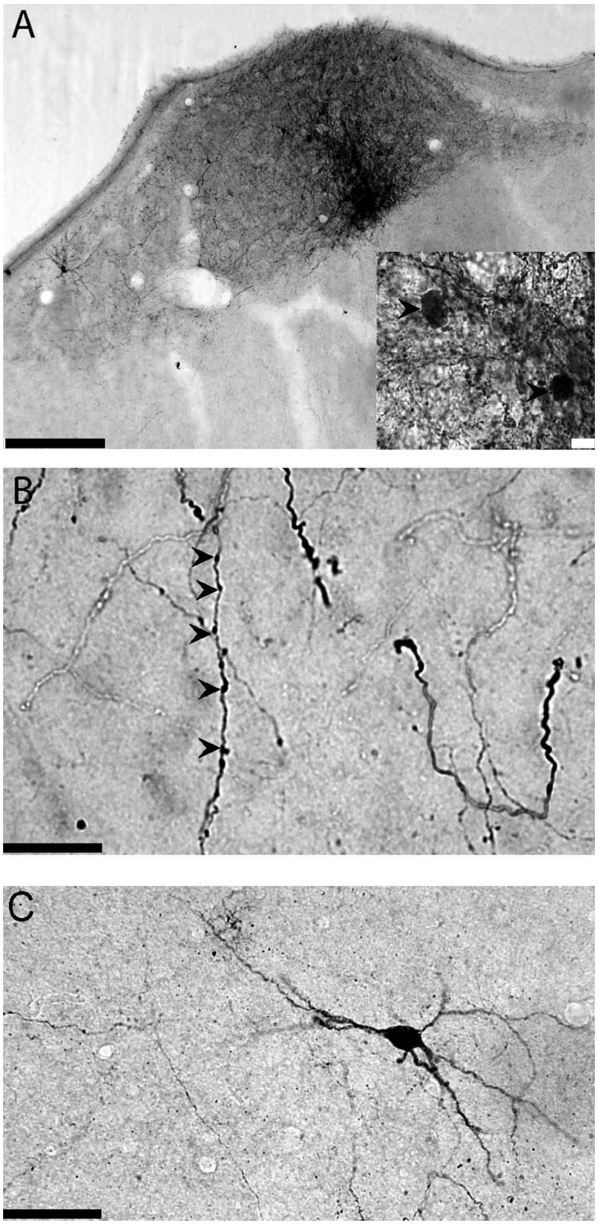

Figure 2.

A: Example of an injection site in HVC. Inset shows several cell bodies in HVC (arrowheads) labeled with BDA. **B:** BDA-labeled HVC_{RA} axon arbors in RA. Examples of varicosities are marked with arrowheads. **C:** Retrogradely labeled cell body in RA following BDA injection in HVC. Scale bars = 100 μm in A; 10 μm in A, inset and B; 50 μm in C.

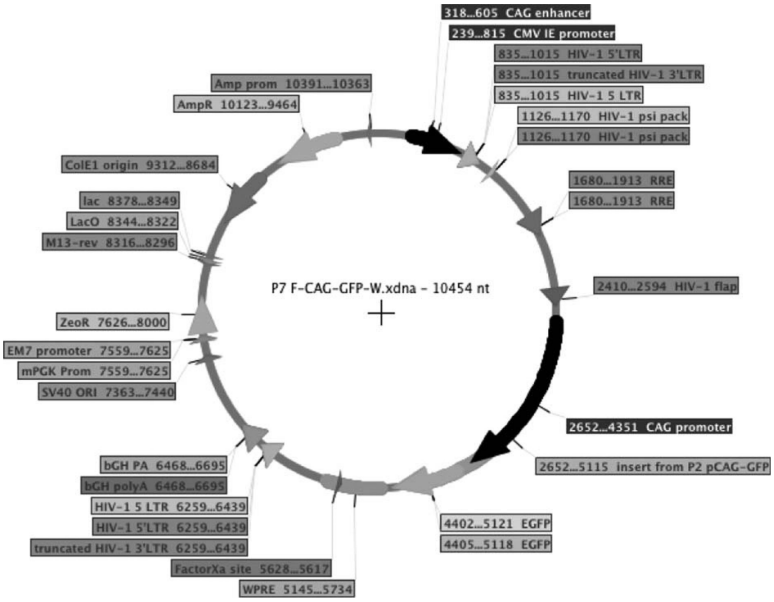

Figure 3.
Vector map of lentivirus used to label neurons in HVC.

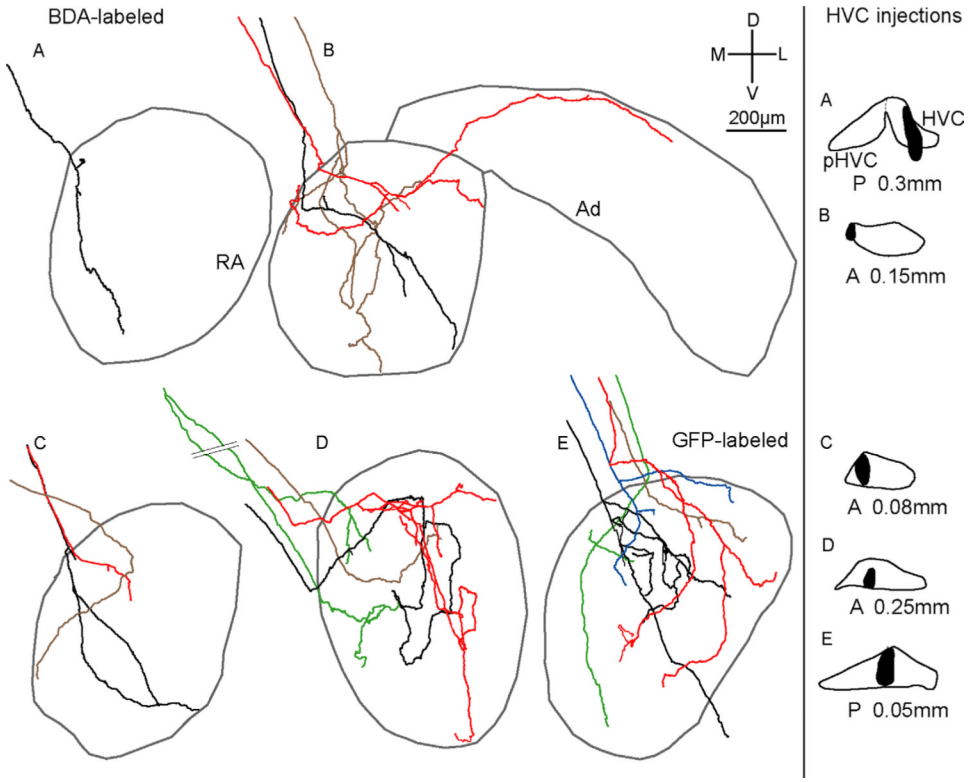

Figure 4.

Reconstructions of all 16 individual HVC axons in RA as a function of injection site. Each color represents a different HVC_{RA} axon. Gray outlines show borders of RA as defined by Nissl staining; gray borders in B also show approximate borders of Ad. **A–D** (Left): BDA-labeled axons (n = 11) in four birds. **E** (Left): GFP-labeled axon arbors (n = 5) in one bird. One axon (B, red) sent a branch into Ad. Right panel: injection sites (black) in HVC for each bird. Injections in A,D were in left HVC, whereas injections in B,C,E were in right HVC; left injections and resultant label in RA are shown as mirror images so that all sections appear as right RA/HVC. We defined the middle of HVC as AP 0.0 for each bird; the A, P values on the right refer to the relative location of the injection site. [Color figure can be viewed in the online issue, which is available at wileyonlinelibrary.com.]

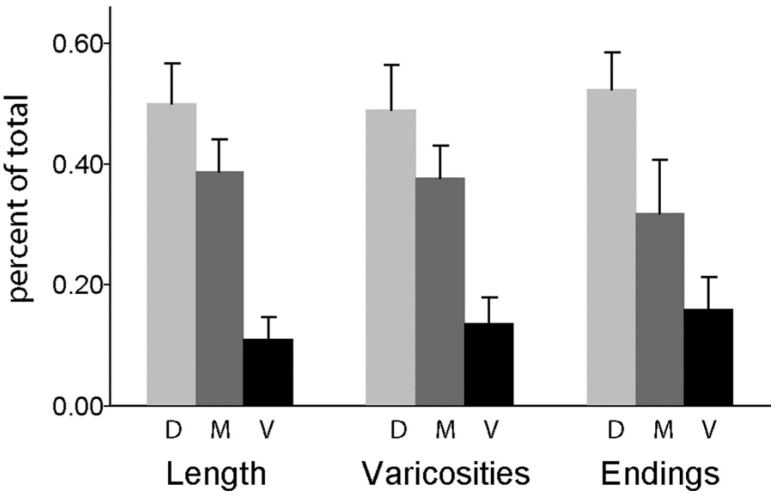

Figure 5.
Proportion of total length, number of varicosities, and number of endings in the dorsal, middle, and ventral third of RA.

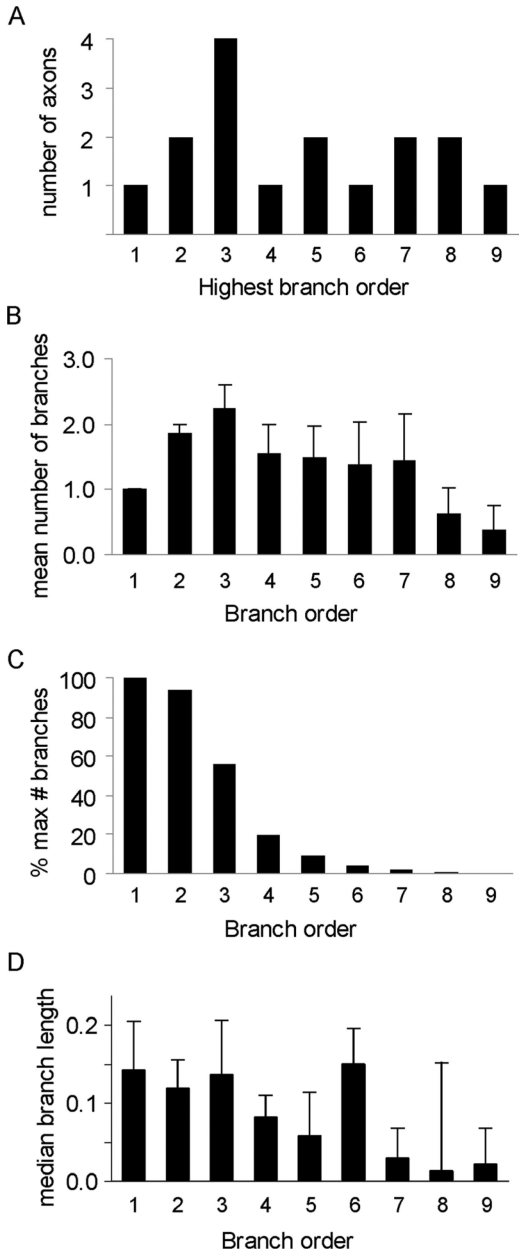

Figure 6.

Number of HVC_{RA} axons, average number of branches, percentage of the maximum number of branches, and median branch length as a function of branch order. **A:** The number of HVC_{RA} axons as a function of highest branch order. **B:** The average number of branches per arbor as a function of branch order. **C:** The number of branches, expressed as a percentage of the maximum number of branches in each branch order, by branch order. **D:** Branch length (mm) of HVC_{RA} axons by branch order.

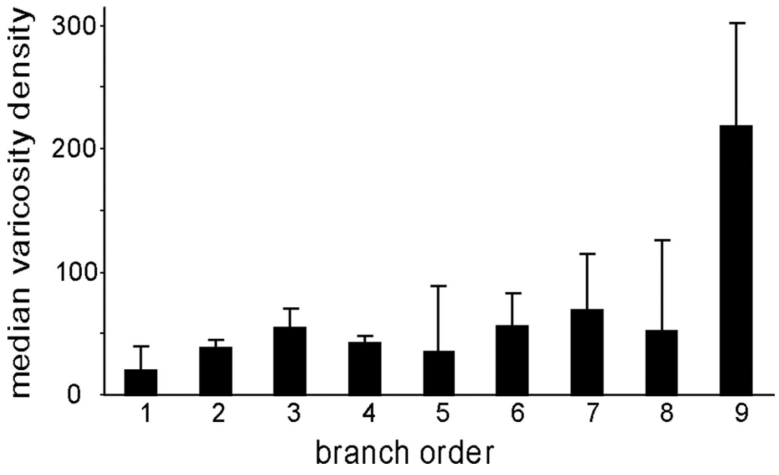

Figure 7.
Varicosity density (number of varicosities/mm) of BDA-labeled axons by branch order.

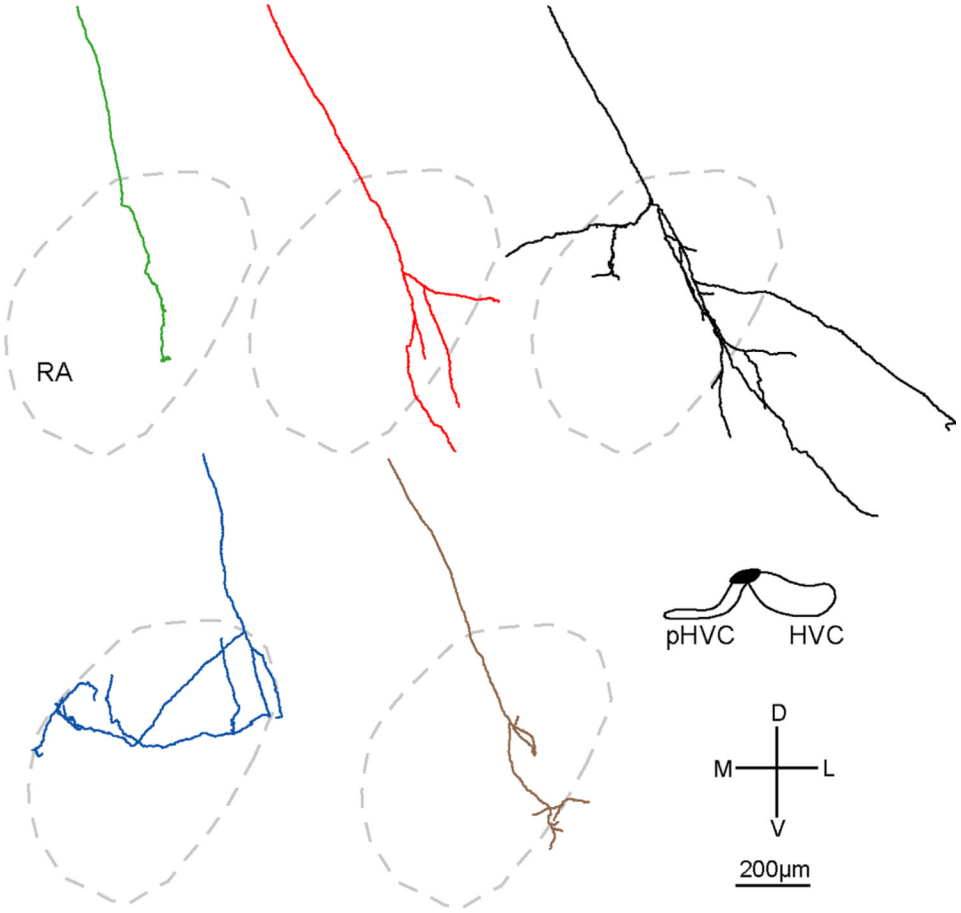

Figure 8.

Reconstructions of individual axons in RA cup (*n* = 5) in one adult male zebra finch. Axons are located anterior to the Nissl-defined borders of RA (outlined in gray). [Color figure can be viewed in the online issue, which is available at wileyonlinelibrary.com.]

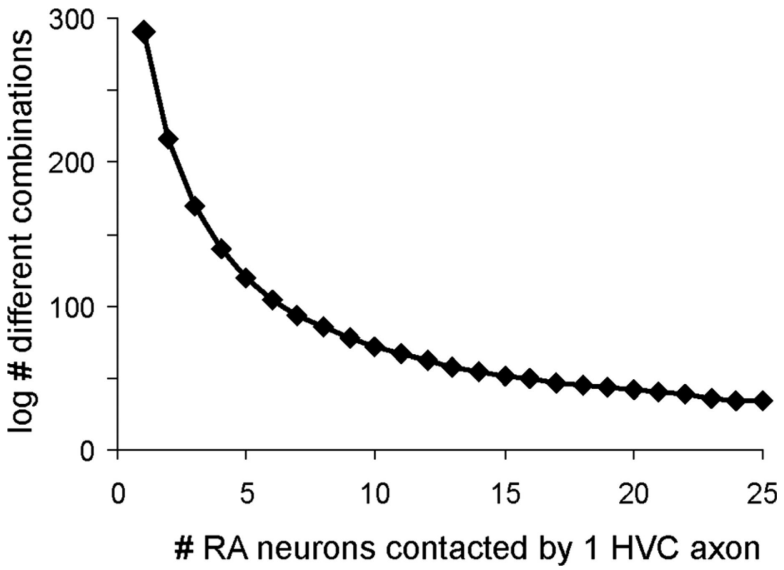

Figure 9.

HVC_{RA} axons with simple morphology increase the number of possible combinations of postsynaptic contacts. We made a simple model in which 400 out of a fixed population of 1,000 RA neurons are required to generate a segment of song. (The number and pattern of mathematical combinations will vary depending on what proportion of RA neurons are activated in order to produce a short segment of sound; our estimate of the proportion of RA neurons activated was intermediate between those of Leonardo and Fee, 2005, and Sober et al., 2008.) If each HVC axon contacts only a single RA neuron, then a very large number of sound combinations can be generated (1,000 choose 400; log value = 291). However, if a single HVC axon contacts four axons then the number of possible combinations drops sharply (1,000 choose 100; log value = 140). Thus, fewer axons with a limited branching pattern are required to activate different combination of RA neurons compared to axons with complex branching patterns. See text.

TABLE 1

Length, Tangential Extent, and Volume of HVC Axon Arbors in RA

	Total length (mm)	Average branch length (mm)	Tangential extent: ML (mm)	Tangential extent: DV (mm)	Tangential extent: AP (mm)	Tangential extent (%): ML	Tangential extent (%): DV	Tangential extent (%): AP	Axon arbor volume (mm^3)	Volume of RA (mm^3)	% of RA occupied
BDA-labeled axons (*n* = 11)	1.63±0.49	0.18±0.07	0.44±0.05	0.55±0.07	0.30±0.04	65.2±6.4	60.4±7.6	38.6±5.7	0.0044±0.004	0.22±0.01	1.60±1.81
GFP-labeled axons (*n* = 5)	1.51±0.85	0.20±0.04	0.39±0.05	0.57±0.11	0.34±0.10	48.7±6.0	61.7±11.8	38.1±11.4	0.0045±0.009	0.24	1.90±3.77
BDA + GFP (*n* = 16)	1.57±0.42	0.19±0.05	0.41±0.03	0.55±0.06	0.32±0.04	53.6±4.8	61.1±6.2	38.3±5.1	0.0045±0.004	0.23±0.01	1.75±1.66

Measures are expressed as median ± SEM. HVC, high vocal center; RA, robust nucleus of the arcopallium; BDA, biotinylated dextran amine; GFP, green fluorescent protein; ML, medial-lateral; DV, dorsal-ventral; AP, anterior-posterior.

TABLE 2

Branching Patterns of HVC Axon Arbors in RA

	Highest branch order	Number of endings	Number of branches
BDA-labeled axons (*n* = 11)	5.0 ± 0.8	6.0 ± 2.1	11.0 ± 4.2
GFP-labeled axons (*n* = 5)	4.0 ± 1.0	4.0 ± 2.0	7.0 ± 3.9
BDA + GFP (*n* = 16)	4.5 ± 0.6	5.0 ± 1.5	9.0 ± 3.1

Measures are expressed as median ± SEM.

TABLE 3

Varicosities of HVC Axon Arbors in RA

	Number of varicosities[‡]	Number of varicosities per branch[†]	Varicosity density (per mm)[*]
BDA-labeled axons (n = 11)	107 ± 20	10.0 ± 4.1	53.9 ± 6.3
GFP-labeled axons (n = 5)	41 ± 21	4.7 ± 1.3	27.0 ± 1.7

Measures are expressed as median ± SEM.

[‡] $P = 0.08$

[†] $P = 0.05$

[*] $P = 0.01$.

TABLE 4

Axon Arbors in RA Cup

	Total length (mm)	Average branch length (mm)	Highest branch order	Number of branches	Number of Varicosities	Number of endings	Number of varicosities per branch	Varicosity density (per mm)
RA cup axons (n = 5)	1.60 ± 0.58	0.23 ± 0.03	4.0 ± 1.0	7.0 ± 3.1	69 ± 46	4.0 ± 1.6	9.9 ± 1.7	41.8 ± 6.4

Measures are expressed as median ± SEM.